Electronic structure of barium-doped C_{60}

Th. Schedel-Niedrig*
Fritz-Haber-Institut der Max-Planck-Gesellschaft, Faradayweg 4-6, D-14195 Berlin (Dahlem), Germany

M. C. Böhm
Institut für Physikalische Chemie, Physikalische Chemie III, Technische Hochschule, Darmstadt, Petersenstraße 20, D-64287 Darmstadt, Germany

H. Werner
Fritz-Haber-Institut der Max-Planck-Gesellschaft, Faradayweg 4-6, D-14195 Berlin (Dahlem), Germany

J. Schulte
Institut für Physikalische Chemie, Physikalische Chemie III, Technische Hochschule, Darmstadt, Petersenstraße 20, D-64287 Darmstadt, Germany

R. Schlögl
Fritz-Haber-Institut der Max-Planck-Gesellschaft, Faradayweg 4-6, D-14195 Berlin (Dahlem), Germany
(Received 4 September 1996)

We have investigated the electronic structure of Ba-doped C_{60} films with Ba concentrations of up to $x \approx 12$ (Ba_xC_{60}) by applying valence-band photoemission and x-ray-absorption spectroscopy. A crystal orbital (CO) formalism based on a semiempirical Hamiltonian of the intermediate-neglect-of-differential-overlap type has been employed to derive solid-state results for the Ba-doped C_{60} fullerides. Using x-ray diffraction, we show three distinct phases for the bulk Ba_xC_{60} system with Ba concentrations of up to $x=6$. In all cases, the experimental observations strongly indicate that fulleride formation leads to the occupation of hybrid bands on both sides of the Fermi level. The theoretical data indicate that the alkaline-earth atoms are essentially monovalent and hybridize strongly with the π-type functions of the C_{60} network. The Ba atoms in the Ba_xC_{60} fullerides deviate from the limit of complete charge transfer as a consequence of the competition between covalent Ba-C_{60} bonding and ionic contributions. Furthermore, it is shown that the calculated density-of-state profiles reproduce the photoemission data in the extreme outer valence-band region. [S0163-1829(97)05020-0]

I. INTRODUCTION

The interesting material properties of alkali- and alkaline-earth-doped C_{60} fullerides such as low-temperature superconductivity have been the subject of numerous research activities. The corresponding results have been published in comprehensive review articles.[1–4] Experimental investigations verified sizeable nonisoelectronic effects with respect to the structural or superconducting behavior.[5,6] It has been demonstrated that most of the known superconducting alkali-doped C_{60} fullerides have the stoichiometry A_3C_{60} or A_2BC_{60} (A,B=alkali atom), form fcc lattices, and are considered to undergo essentially complete charge transfer (CT) from the alkali atoms A,B to C_{60} within a rigid-band model.[7,8] Therefore, all of these alkali-doped C_{60} fullerides show similar electronic-structure properties. Their half-filled valence band is mainly formed by the C_{60}-derived t_{1u} orbital. Superconductivity has also been observed in some alkaline-earth (AE)-doped C_{60} fullerides, Ca_5C_{60} (Ref. 9) and Ba_6C_{60},[10] for example. As a consequence these compounds have been most widely studied.[11,12] In contrast to the alkali-doped A_3C_{60} compounds, theoretical investigations of stoichiometric Ca_nC_{60} phases indicated that substantial hybridization of carbon and calcium orbitals in the valence-band region occurred.[13,14] The exact stoichiometry of the Ba-doped superconducting fulleride still seems to be open.[14] Recently, synthesis of a crystalline, stoichiometric Ba-doped C_{60} superconductor, Ba_6C_{60} with $T_c=7$ K has been reported.[10] Naive electron counting, assuming divalent Ba and the rigid K_6C_{60}-like band structure, would suggest that this compound is a 0.2-eV-gap insulator that contains very highly charged C_{60}^{12} molecules. Photoemission studies of AE_xC_{60} fullerides (AE=Ca,Ba) have shown that doping beyond $x \cong 3$ resulted in the occurrence of electronic states of the alkaline-earth donors in the occupied band region within a few electron volts of the Fermi level $\mathcal{E}_F$.[15–17] Theoretical models[13,14] predict strong Ba-C hybridization near the Fermi level, incomplete charge transfer, and an insulating band-structure[14] with a small gap within the local-density approximation. In a recent photoemission study of the valence band of the AE fullerides Sr_xC_{60} and Ba_xC_{60}, it has been found that these compounds are metallic for AE concentrations up to 6 due to the formation of a hybrid conduction band.[18]

It is the purpose of this paper to investigate the electronic structure of the Ba-doped C_{60} fullerides by applying surface-sensitive spectroscopic methods, namely, valence-band photoemission and x-ray absorption under clean ultra-high-vacuum (UHV) conditions and, on the other hand, a band-structure model based on an intermediate-neglect-of-differential-overlap (INDO) Hamiltonian.[19] From detailed

experimental studies it is well known that alkali- and alkaline-earth-doped fullerides are in the neighborhood of metal-insulator transitions.[20,21] Therefore, we have also studied a Mott like insulating configuration in Ba_5C_{60}.

The outline of the present paper is as follows. In Sec. II, the preparation conditions of the film (Sec. II A) and bulk (Sec. II B) fullerides are given. A short description of the experimental techniques applied is made in Sec. III C. The computational conditions of the CO calculations are described in Sec. II D. The crystal structures based on the x-ray diffraction (XRD) results are commented on in Sec. III. A representation and discussion of the experimental (Sec. IV A) and theoretical (Sec. IV B) results is given in Sec. IV. The contribution ends with some concluding remarks in Sec. V.

II. EXPERIMENTAL AND THEORETICAL DETAILS

A. Preparation of thin films

The C_{60} powder was prepared by the electric-arc method, purified by column chromatography (toluene-active carbon-silica gel-alumina) and checked for phase purity by UV-visible and infrared (IR) spectroscopy and analytical high pressure liquid chromatography. It was then sublimed from a Knudsen cell furnace onto clean Pt-substrate surfaces (foil, 99.95% purity) held at 300 K in a UHV preparation chamber. Subsequently, the C_{60} films were exposed to a flux of Ba at 300 K substrate temperature, which was also sublimed from a Knudsen cell furnace in the preparation chamber. After thorough degassing, Ba deposition could be done at pressures below 2×10^{-9} mbar. After Ba deposition, the films were heated to 620 K (Pt-substrate temperature) for $\sim$15 min in order to enhance the Ba-C_{60} mixing. The amount of material deposited was determined with a quartz-crystal-thickness monitor. The Ba-C_{60} stoichiometries were determined by monitoring the Ba $3d_{5/2}$ and the C 1*s* core-level intensities with x-ray photoelectron spectroscopy (XPS) using the nonmonochromatized Mg $K\alpha$ radiation ($h\nu$ = 1253.6 eV). Surface compositions were determined after substraction of a Shirley-type background using the cross sections from Ref. 22. Since the mean free path for these electrons was $\sim$15 Å in the Ba_xC_{60} films, about 95% of the signal came from within $\sim$45 Å of the surface. The stoichiometry uncertainty, approximately $\pm$15% in these studies, reflects systematic errors in determining the intensities of the C 1*s* and Ba $3d_{5/2}$ main line and satellite structures and uncertainties related to the electron mean free path in Ba_xC_{60}. These XPS measurements allowed us to calibrate the stoichiometries of the films obtained under identical growth conditions in photoemission and x-ray-absorption studies.

B. Preparation of bulk samples

The C_{60} starting material was purified, dried, and afterwards transferred into an Ar-filled glove box together with Ba lumps. These lumps were filed to obtain Ba powder, since commercially available Ba powders contain oxidic contaminations. Stoichiometric amounts of Ba and C_{60} powder were mixed, pelletized, and sealed in an evacuated quartz ampoule to enhance the grain contact during the solid-state reaction, which was carried out at 700 K for five days. Unfortunately, Ba tends to react with the ampoule material to form silicides and oxides at temperatures above 650–700 K. At still higher temperatures, barium carbides are also formed. These possible reactions determine the applied-temperature limit during the preparation of the bulk samples. After this high-temperature and long-term treatment, the new fulleride phase exhibited metallic luster and was brittle. Using x-ray diffraction, the main compounds were determined to be Ba_6C_{60} (main component), Ba_3C_{60}, an additional phase of unspecified stoichiometry (Ba_xC_{60} phase, see Sec. III), and small BaO contaminations ($\sim$1%). Therefore, the Ba_6C_{60} compound was used as a precursor material for Ba concentrations of $x<6$. For this purpose Ba_6C_{60} was mixed with the desired amount of pure C_{60} powder and was afterwards treated in the same manner as described above.

C. Experimental methods

Valence-band and core-level photoemission, ultraviolet photoemission spectroscopy (UPS) and XPS, as well as x-ray absorption spectroscopy (XAS) were carried out in a vacuum-generator (VG) double-chamber UHV system with a base pressure of $<1\times10^{-10}$ mbar. The XPS source was the nonmonochromatized Mg $K\alpha$ line (1253.6 eV) and the instrumental broadening is estimated to be 0.9 eV for XPS. A VG CLAM100 electron-energy analyzer was used for the photoemission experiments and a partial-electron-yield detector for XAS. In the UPS studies, He I radiation ($h\nu$ = 21.2 eV) was used. The UPS measurements were done at 300 K, giving an overall resolution of 200 meV, as determined from the Fermi edge of a clean polycrystalline Pt surface. The energy positions and the intensities of the valence-band structures were determined by fitting each with a combined Lorentzian/Gaussian function. The zero binding energy (BE) of the UPS data was referenced to the Fermi edge of a clean Pt foil.

The XAS measurements were performed at the SX-700I beamline of the Berliner synchrotron radiation source (BESSY). The synchrotron-radiation photon energy ranges from 10 to 2000 eV and the monochromator was operated with a resolution of 0.5 eV at the C *K* edge. The photon energy was calibrated to an accuracy of $\pm$0.5 eV with reference to the La $3d\rightarrow4f$ transition of a $LaAl_2$ sample at 836 eV. The XAS data were collected in the partial-yield mode with a retarding voltage of $-$200 V. To avoid problems with the spectral artifacts of carbon contamination of optical components, the spectra were divided by the spectrum from a clean Cu(110) surface recorded under the same conditions and were subsequently normalized to the edge jump.

X-ray diffraction was carried out with Cu $K\alpha$ radiation using STOE STADI P diffractometers [double circle diffractometer equipped with a Ge(111)-primary monochromator]. High-resolution data were collected in the focusing Debye-Scherrer transmission geometry with samples sealed in Lindemann tubes in a glove box under Ar.

D. Computational conditions of the crystal-orbital calculations

The theoretical background of the crystal-orbital (CO) method employed has been described in Ref. 19. The method is based on a semiempirical Hamiltonian of the INDO type. We have approximated the atomic parameters of Ba using Ca elements that have been inserted into the present CO Hamil-

TABLE I. Number of **k** points considered in the irreducible part of the Brillouin zone (BZ) and the total BZ in the crystal orbital calculations of Ba_xC_{60} fullerides.

System	**k**-grid IBZ	**k**-grid BZ
Ba_3C_{60}	10	240
Ba_4C_{60}	54	216
$Ba_5C_6O(1)$	22	264
$Ba_5C_{60}(2)$	56	216
Ba_6C_{60}	14	168

tonian. To simulate the effect of the larger atomic radius of Ba relative to Ca, we have adopted the screening coefficients ξ of K. Note that the covalent and ionic radii of Ba and K are roughly the same. In contrast to the majority of solid-state electronic-structure investigations of fullerenes and fullerides, which are based on variants of the density-functional method, the present CO formulation corresponds to an approximation to the Hartree-Fock equations. For earlier applications of the present CO method to fullerenes, refer to Refs. 23–26. The capability and also the limitations of the method in connection with nonfulleride solids with large unit-cell dimensions have been shown in a series of CO investigations.[27–30] The application of the INDO CO approach makes it necessary to divide the total crystal volume into two types of spatial domains I and II.

Domain I defines an atomic sphere with radius R_S which has to be defined for any atomic site. In these spheres the self-consistent-field (SCF) equations in a basis of Bloch orbitals are solved exactly in the given theoretical degree of sophistication. In the remaining crystal volume, i.e., domain II, the two-center interaction is approximated by the classical Madelung potential. Model calculations as a function of the atomic-sphere radius R_S have shown that a R_S value of 7.0 Å is a reliable compromise between numerical accuracy of the method on the one hand and computer time and storage demand on the other.[31] In the numerical integration of the charge-density bond-order matrices, we have used the discrete summation. The convergence properties of different numerical integration techniques in CO calculations have been investigated in Ref. 32. For the generation of the **k** grids, **k** is the conventional wave vector in the electronic theory of solids, we have adopted a generalization of the so-called large-unit-cell method.[33] The present approach makes use of the Patterson symmetry in reciprocal space.[34] For most of the Ba_xC_{60} solids studied in this work, by crystal-orbital calculations, the Patterson symmetry coincides with the space-group symmetry. An exception is Ba_3C_{60}, where the space-group symmetry is Pm3n (see Sec. III) while the Patterson symmetry is Pm3m. It is the conceptual advantage of the present **k** integration that the underlying spatial domains are of simpler geometric structure than those of the standard Brillouin zones (BZ's). In Table I we have summarized the number of **k** points considered in the irreducible part of the BZ and in the total BZ. The **k** arrays employed in the present CO calculations exceed the dimension of **k** arrays used in many previous band-structure calculations of fullerides. In the post-SCF part, i.e., in the construction of the energy bands $\varepsilon_i(\mathbf{k})$ and the electronic density-of-states (DOS) distribution, we have enlarged the **k** grid relative to those given in Table I. The labels of Miller and Love[35] have been used to classify the symmetry directions and symmetry points in reciprocal space. A standard histogram technique has been used to evaluate the DOS profiles. In this step, we have adopted a width of 0.2 eV. In a second step, the DOS histograms have been smoothed by Gaussian functions with a mean width of 0.35 eV. To stabilize the SCF iterations we have adopted a Hartree damping of the bond-order matrices.

In most of the Ba_xC_{60} systems considered, we have found insulating (semiconducting) electronic configurations with a gap between filled and empty dispersion curves $\varepsilon_i(\mathbf{k})$. Only in the case of $Ba_5C_{60}(1)$, i.e., in the solid-state geometry which has been extrapolated from Ca_5C_{60} (see Sec. III), did the INDO CO approach converge to a metallic solution with a partially filled conduction band. From detailed experimental investigations, it is well-known that alkali- and alkaline-earth-doped fullerides are in the neighborhood of metal-insulator transitions.[20,21] With these materials one has a strong competition between metallic configurations and insulating configurations of the Mott type, where the number of singly occupied **k** states corresponds to a maximum.[36] Exchange of the alkali- or alkaline-earth donor for another one and the accompanying changes in the unit-cell dimension are often sufficient to cause a transition from a metal to a Mott-type insulator or vice versa. Therefore, we have studied a Mott-like configuration in $Ba_5C_{60}(1)$ as well. In recent contributions, we have demonstrated that the present INDO CO approach is a rather useful tool for discussing this problem in a one-determinantal approximation.[24,25,37] For INDO CO calculations, treating the competition between metallic and Mott-like states in fullerides, see Refs. 24 and 25. The theoretical background of CO calculations of Mott configurations has been described in Ref. 37. The CO computations have been performed on the SNI S400/40 supercomputer at the Rechenzentrum of the Technische Hochschule Darmstadt and on a silicon graphics workstation of the type Power Onyx. For Ba_3C_{60} with $z=2$ about 8 hs of CPU time are necessary on the SNI 400/40 supercomputer (z stands here for the number of formula units per unit cell). The CPU time demand at the work station for the same $z=2$ solid exceeds 24 hs. The other CO calculations of Ba_xC_{60} fullerides with $z=1$ required roughly one hour of CPU time on the SNI 400/40 computer. The space demand of the INDO CO program is about 1 Gbyte. Finally we want to mention that we have 126 atoms corresponding to 504 atomic orbitals per unit cell in the Ba_3C_{60} calculation. In the basis of Bloch orbitals this leads to a Hermitian eigenvalue problem of dimension 1008×1008. To the best of our knowledge, band-structure calculations on the SCF level for such large unit cell dimensions have not been published up to now.

III. CRYSTAL STRUCTURE

Three phases have been observed with XRD for the Ba_xC_{60} system as shown in Fig. 1: for $0<x<3$ the material has been a mixture of C_{60} and simple cubic Ba_3C_{60}.[10] For $3<x<6$ we observed a mixture of Ba_3C_{60} and Ba_6C_{60} (Ref. 38) and found strong evidence for another new phase in this range of composition. The largest abundance of this new phase has been been observed for a nominal composition of Ba_4C_{60}.

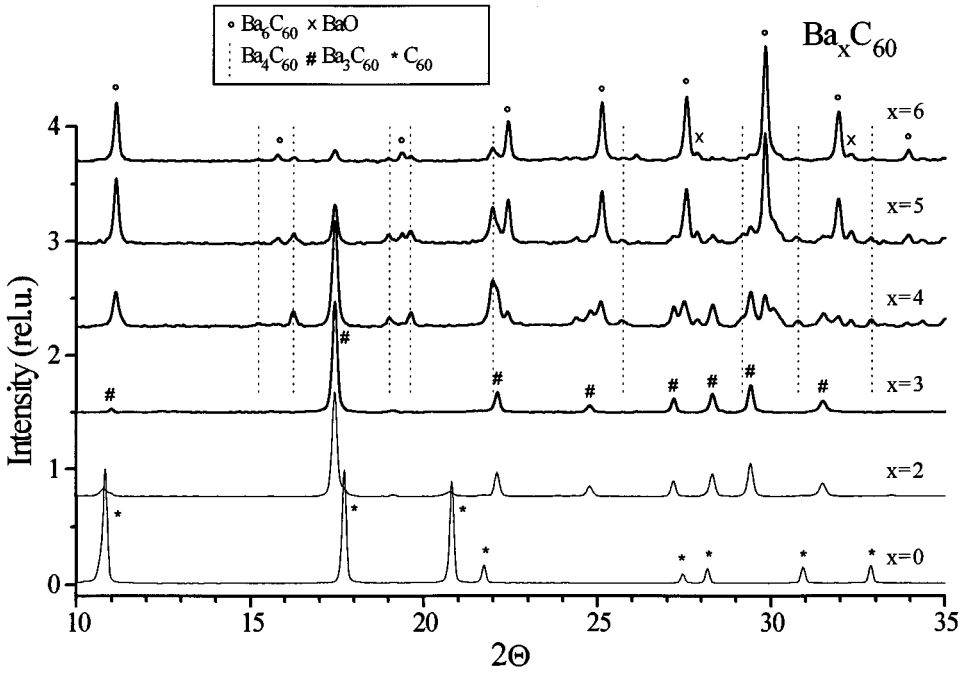

FIG. 1. X-ray diffraction data of the Ba-doped C_{60} bulk phases with Ba concentrations of $x=2$, 3, 4, 5, and 6.

TABLE II. Space groups (SG), Bravais lattices (BL), unit-cell dimension a,b,c (in Å), and Ba positions in fractional coordinates in Ba_xC_{60}. Ba_3C_{60} has been calculated with $z=2$ formula units per unit cell. For Ba_5C_{60} two different solid-state geometries, i.e., $Ba_5C_{60}(1)$ and $Ba_5C_{60}(2)$, have been considered. The lattice constants of the fullerides with Ba concentrations of $x=3$, 4, and 6 are determined by XRD.

System	SG	BL	a	b	c	x	y	z
Ba_3C_{60}	$Pm\bar{3}n$	sc	11.343			0.25	0.00	0.50
						0.50	0.25	0.00
						0.00	0.50	0.25
						0.75	0.00	0.50
						0.50	0.75	0.00
						0.00	0.50	0.75
Ba_4C_{60}	Immm	bco	11.250	11.600	10.900	0.22	0.50	0.00
						0.50	0.28	0.00
						0.50	−0.28	0.0
						−0.22	0.50	0.00
$Ba_5C_{60}(1)$	$Fm\bar{3}$	fcc	14.198			0.25	0.25	0.25
						0.40	0.40	0.40
						−0.40	−0.40	0.40
						−0.40	0.40	−0.40
						0.40	−0.40	−0.40
$Ba_5C_{60}(2)$	Immm	bco	11.171	11.171	11.171	0.50	0.28	0.00
						0.50	−0.28	0.00
						0.28	0.00	0.50
						−0.28	0.00	0.50
						0.00	0.50	0.28
Ba_6C_{60}	$Im\bar{3}$	bcc	11.171			0.50	0.28	0.00
						0.50	−0.28	0.00
						0.28	0.00	0.50
						−0.28	0.00	0.50
						0.00	0.50	0.28
						0.00	0.50	−0.28

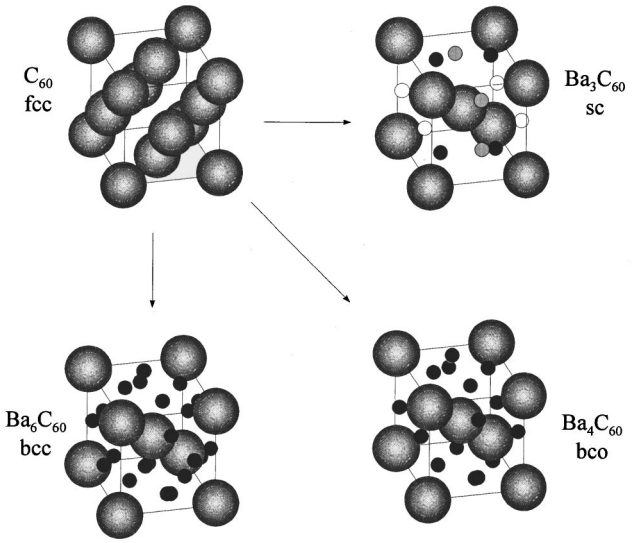

FIG. 2. The structures of pristine and Ba-doped C_{60} as determined by XRD. The structure of solid C_{60} is a fcc cell as shown on the upper left-hand panel. There are three interstitial sites available per C_{60} unit for intercalated alkaline-earth-metal atoms: Two of the sites provide tetrahedral coordination (four nearest C_{60} neighbors), and one allows octahedral coordination (six nearest C_{60} neighbors). For stoichiometries equal to or greater than three Ba atoms per C_{60}, the crystal expands and transforms to different structures: A simple cubic (sc) structure for Ba_3C_{60} (upper right-hand panel) with three equivalent Ba positions as indicated (Ref. 39), a bco structure for Ba_4C_{60} (lower right-hand panel), and a bcc structure for Ba_6C_{60} (lower left-hand panel).

The lattice constants of Ba_4C_{60} could not be determined with the same accuracy as for Ba_3C_{60} and Ba_6C_{60} (see Table II) due to the low intensity and the strong overlap with the reflections of the Ba_3C_{60} phase. For the same reason, it was not possible to perform a Rietveld analysis. We propose a body-centered orthorhombic structure for the new phase with approximately the same arrangement of C_{60} as encountered in the unit cells of Ba_3C_{60} and Ba_6C_{60} (see Fig. 2). This phase can be derived either from the Ba_3C_{60} phase with partial filling of the unoccupied interstitial sites or from the Ba_6C_{60} phase with partial deoccupation of the filled sites (see Fig. 2). Hence, similar to fullerides of heavier alkali metals (A) we suggest a compound of the A_4C_{60} type (Fig. 2) with a different lattice due to a favored occupation of voids faced by the five-membered rings of the fullerenes as proposed by Kortan *et al.*[10]

In the crystal orbital (CO) Sec. IV B of the present contribution, we have considered four Ba_xC_{60} stoichiometries, i.e., Ba_3C_{60}, Ba_4C_{60}, Ba_5C_{60} in two different solid-state structures as well as Ba_6C_{60}. In Table II we have summarized the corresponding space groups (SG's), the Bravais lattices (BL), the unit cell dimensions, and the atomic positions of Ba in terms of fractional coordinates. The data of the table have been used as input in the band-structure calculations.

The existence of at least one additional phase between the unambiguously identified Ba_3C_{60} and Ba_6C_{60} phases has been commented on above.[38] It was assigned to Ba_4C_{60}. Nevertheless, we have studied the stoichiometry of Ba_5C_{60} as well. Since structural information is not available for this stoichiometry, we have adopted two plausible structures in the CO calculations. In the following they are denoted as $Ba_5C_{60}(1)$ and $Ba_5C_{60}(2)$. Let us start with a short description of the Ba_3C_{60} structure. In contrast to alkali-doped A_3C_{60} fullerides which crystallize in a fcc lattice with two tetrahedral (t) and one octahedral (o) interstitial site, Ba_3C_{60} forms an A15 structure with three equivalent alkaline-earth positions.[39] The unit cell is primitive cubic (see Fig. 2). In Sec. II D, we have mentioned already that two formula units of Ba_3C_{60} are required to define the unit cell. The centers of the C_{60} molecules form a bcc lattice. The Ba atoms are tetrahedrally coordinated by the five-membered rings of the C_{60} soccer balls. An orthorhombic Bravais lattice with space-group Immm has been selected for the phase Ba_4C_{60} (Ref. 39) (see Fig. 2). Note that this space-group symmetry coincides with the one realized in alkali-doped A_4C_{60} fullerides.[40,41] Ordered C_{60} molecules in Ba_4C_{60} force a crystal symmetry which is no higher than body-centered orthorhombic (bcc). Ordering of the C_{60} units is incompatible with the higher I4/mmm symmetry because a fourfold axis is missing in the C_{60} molecule. The C_{60} molecules must be orientationally disordered for Ba_4C_{60} to be body-centered tetragonal (bct). The Ba positions in Ba_4C_{60} correspond to distorted tetrahedral sites. Before describing the Ba_5C_{60} crystal structures selected, we want to introduce the Ba_6C_{60} structure. This alkaline-earth-doped C_{60} fulleride crystallizes in a bcc lattice with distorted tetrahedral interstitial sites occupied by Ba atoms.[10] The same structure is realized in A_6C_{60} alkali-doped C_{60} fullerides with heavier alkali atoms. The orientation of the C_{60} soccerball determines the space-group symmetry; possible candidates e.g., are Im3 or Im3m. Finally, we introduce the two Ba_5C_{60} structures selected on the basis of x-ray data observed for Ca_5C_{60}[40] or extrapolated from Ba_6C_{60}.[10] Model 1 [i.e., $Ba_5C_{60}(1)$] corresponds to the Ca_5C_{60} structure which crystallizes in a fcc lattice. In the calcium phase four Ca atoms form some kind of Ca_4-tetrahedron with origin at the o position of the fcc lattice. In the corresponding Ba_5C_{60} model this arrangement leads to Ba-Ba distances in the ''Ba_4 tetrahedron'' of 3.69 and 4.02 Å. The fifth alkaline-earth atom is located at one of the two t positions. The second interstitial t site remains unoccupied. $Ba_5C_{60}(2)$ has been derived from Ba_6C_{60} with one distorted tetrahedral site unoccupied. In all CO calculations we have conserved a common geometry of the C_{60} soccerball. This choice allows us to study modifications in the C_{60} solid-state electronic structure as a function of the Ba-to-C_{60} charge transfer and intermolecular spatial-degrees of freedom. The C_{60} diameter adopted amounts to 7.06 Å. Furthermore, we have employed the experimental bond-length alternation between six-ring-six-ring [=(6-6)] and six-ring-five-ring [=(6-5)] bonds of undoped C_{60}. Here the (6-6) bonds have a length of 1.396 Å while the bond length of the (6-5) bonds amounts to 1.439 Å.[41]

IV. RESULTS AND DISCUSSION

A. Photoemission and x-ray absorption

Figure 3 shows a series of the valence-band photoemission spectra of Ba-doped C_{60} films as a function of the Ba concentration x. The binding energies are referenced to the Fermi level ε_F of the clean Pt substrate surface and the in-

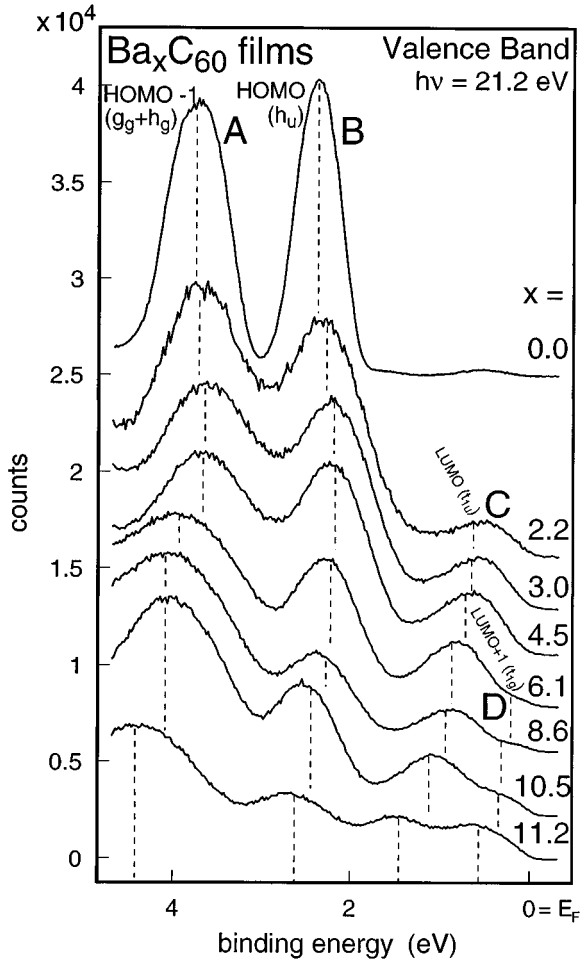

FIG. 3. Photoemission valence-band spectra of Ba-doped C_{60} films for Ba concentrations of x ranging between 2.2 and 11.2 (taken with $h\nu = 21.2$ eV photon energy). The top spectrum shows the valence band of a 1000-Å-thick pristine C_{60} film.

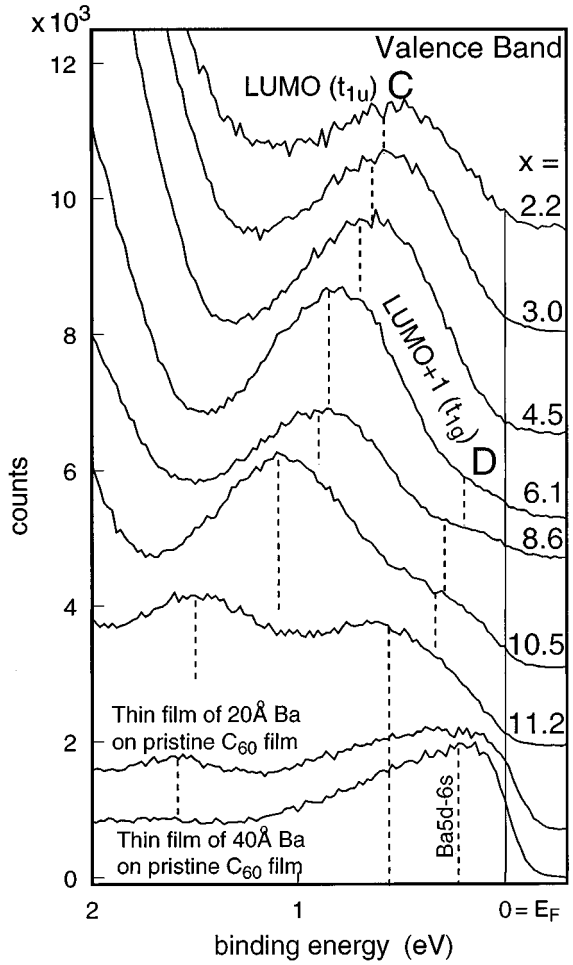

FIG. 4. Development of the LUMO (t_{1u}) and LUMO+1 (t_{1g})-derived valence bands, *C* and *D*, as a function of Ba doping of the C_{60} films. The Fermi level does not fall within the LUMO (t_{1u})-derived band *C* up to a Ba concentration of $x = 4.5$, indicating that the fulleride is *semiconducting* or *insulating*. The filling of the LUMO (t_{1u}) -derived band *C* appeared to be complete at $x = 3.0$ and it is not cut by the Fermi level. Another LUMO+1 (t_{1g}) -derived band *D* starts to grow above the LUMO band *C* beginning at doping concentrations of $x = 6.1$ and the band was cut by the Fermi level for doping levels of $x \geq 8.6$, giving rise to a *semimetallic* or *metallic* fulleride. The bottom spectrum for a 40 Å-thick Ba film on a thick pristine C_{60} film shows Ba 5*d*-6*s* hybrid states near the Fermi level. The bottom, minus one spectrum for a 20 Å Ba film deposited on clean C_{60} without subsequent annealing shows the Ba 5*d*-6*s* hybrid states and the LUMO (t_{1u}) and LUMO+1 (t_{1g}) -derived bands, *C* and *D*, from the Ba-C_{60} interface layer.

tensity scale is held constant so that changes in peak heights reflect changes in the photoyield. The top curve is for a 1000-Å-thick pristine C_{60} film. The two peaks at 2.4 eV (labeled *B*) and 3.8 eV (labeled *A*) BE below the Fermi level are caused by π functions (with some σ admixtures[25]) of h_u and $g_g + h_g$ symmetry. The weak peak near 0.5 eV BE seen in the C_{60} spectrum is mainly due to the photoemission from the highest occupied molecular orbital (HOMO) h_u band stimulated by He I satellite radiation ($h\nu = 23.1$ eV, 5–10%). The second curve corresponding to $x = 2.2$ shows broadening and shifting towards ε_F of the HOMO (h_u) and HOMO-1 ($g_g + h_g$) -derived peaks *B* and *A*. Additionally, we observe that the concentration of Ba has created a new band centered 1.6 eV (labeled *C*) above the HOMO (h_u) peak of C_{60} of 0.6 eV BE that can be assigned to the lowest-unoccupied-molecular-orbital (LUMO) t_{1u} band of C_{60}. As the Ba concentration is further increased by evaporation and annealing, the new band *C* begins to grow and to shift to higher BE, while the HOMO (*B*) and HOMO-1 (*A*) peaks further shift towards ε_F. The development of the new LUMO-derived band *C* is shown in Fig. 4. It can be seen that up to a Ba concentration of $x = 4.5$, the Fermi level does not fall within this band, indicating that the fulleride is *not metallic*. The filling of the band *C* appears at $x = 3.0$ to be complete and another band (labeled *D*) begins to grow above this LUMO band *C* for Ba concentrations of $x \geq 6.1$. For the $Ba_{(x=4.5)}C_{60}$ compound, the band *C* appears at somewhat higher BE (0.7 eV) and exhibits an increased peak height. The $Ba_{(x=3.0)}C_{60}$ fulleride is *not metallic*, since there is *no* photoemission at the Fermi level, a result that is in agreement with the photoemission results of Knupfer *et al.*[17] but is in contrast to the photoemission data of Chen *et al.*[18] X-ray analysis for Ba_xC_{60} suggests a mixture of fcc C_{60} ($a = 14.17$ Å) and simple cubic Ba_3C_{60} ($a = 11.343$ Å) for $0 < x < 3$. There is some evidence for a bcc phase for Ba_4C_{60} ($a = 11.25$, $b = 11.60$, $c = 10.90$ Å) (see Table II).

Further deposition and annealing results in a shift of the LUMO (t_{1u}) *C*, HOMO (h_u) *B*, and HOMO-1 (g_g+h_g) *A*-derived bands to higher BE's. It produces a second new band (labeled *D*) for Ba concentrations of $x=6.1$ at 0.2 eV BE (centered 2.0 eV above the HOMO (h_u) -derived band *B*, see Fig. 3). The corresponding band *D* is probably cut by the Fermi level. X-ray analysis for Ba_6C_{60} suggests a bcc phase with a lattice constant of 11.171 Å (see Table II). A clear Fermi-level cutoff has been found for Ba_6C_{60} in a recent photoemission study.[17] Additional Ba deposition leads to the filling of this band *D* and shifts the valence-band features ($A-C$) to higher BE. The highest Ba concentration achieved for Ba_xC_{60} was $x=11.2$. At this stoichiometry, the HOMO (h_u) peak *B* was 0.5 eV larger in BE than for $x=3.0$ and appears 0.2 eV above the HOMO (h_u) band of the pristine C_{60} (see Fig. 3).

The region near the Fermi level (see Fig. 4) shows that the fulleride films up to Ba concentrations of $x=4.5$ likely exhibit a semiconducting or insulating behavior. For $x=6.1$ they probably become a semiconductor and a semimetal for Ba concentrations exceeding 8.6. We have observed that the LUMO+1 (t_{lg}) -derived band *D* was cut by the Fermi level. Only weak photoemission at the Fermi level is observed for the highest Ba concentration of $x=11.2$, suggesting that the fulleride film probably becomes semiconducting or insulating again. The new band *D* cut by the Fermi level can be attributed to the filling of a hybrid band derived from the LUMO+1 (t_{lg}) band of C_{60} and the $5d$-$6s$ states of the Ba atoms (see the theoretical results summarized in Sec. IV B).

The shift of the π-derived [HOMO (h_u) *B* and HOMO-1 (g_g+h_g) *A*] bands in the fulleride films up to Ba concentration of $x=4.5$ (*A* band) and $x=8.6$ (*B* band) towards lower BE values relative to the peak positions of the undoped C_{60} film can be interpreted via the increasing excess charge on the C_{60} soccer ball as discussed in more detail in the band-structure Section (IV B). On the other hand, we observe a shift of these bands in the fulleride films towards higher BEs for Ba concentrations of $x=10.5$ and 11.2, indicating that a second and energetically stabilizing effect occurs simultaneously and exceeds the first and energetically destabilizing effect at higher Ba concentrations. It has most recently been found in a band-structure model of the C_{60} fragment in alkali- and alkaline-earth-doped fullerides[42] that some kind of electronic switch is activated with an increasing population of the LUMO (t_{1u}) and LUMO+1 (t_{1g}) π^*-derived bands, which results in an interconversion of the bonding character of the hexagon-hexagon and hexagon-pentagon bonds under conservation of the overall π bonding. The growing widths of the photoemission features with Ba doping can be due to an increase of the amplitudes of the zero-point vibrations in the C_{60} unit as a response to the Coulomb repulsion between the charged carbon atoms (see Sec. IV B).

Deposition of Ba atoms onto the surface of pristine C_{60} or Ba_xC_{60} film *without* subsequent annealing results in the formation of metal clusters (or islands) on the C_{60}-fulleride surface. They can be identified via the characteristic line shapes of metallic Ba $3d$ core-levels (not shown). This suggests that annealing is required because of the large activation energies for diffusion. The bottom curve in Fig. 4 is a spectrum of a 40 Å Ba film deposited onto a pristine C_{60} film prior to annealing which shows good agreement with the corresponding valence band of a clean Ba surface;[43] the curve exhibits the Ba $5d$-$6s$ hybrid states near the Fermi level. The LUMO+1 (t_{1g}) (*D*; as a shoulder) and LUMO (t_{lu})-derived (*C*) bands of the fulleride can be observed at ~0.7 and 1.6 eV BE in the bottom, minus one spectrum of Fig. 4 for a 20 Å Ba film deposited onto a pristine C_{60} film (without subsequent annealing) indicating that a Ba concentration of $x\geqslant 11$ is obtained at the Ba-C_{60} interface. This suggests that the interface layer is enriched relative to the interior with a possible conversion to a phase of $Ba_{x\geqslant 11}C_{60}$ and it can be assumed that this layer acts as a kinetic barrier so that thermal activation is necessary to form homogeneous macroscopic films. An O $2p$-derived state as observed in Ba oxide films[43] at ~4.7 eV was not observed.

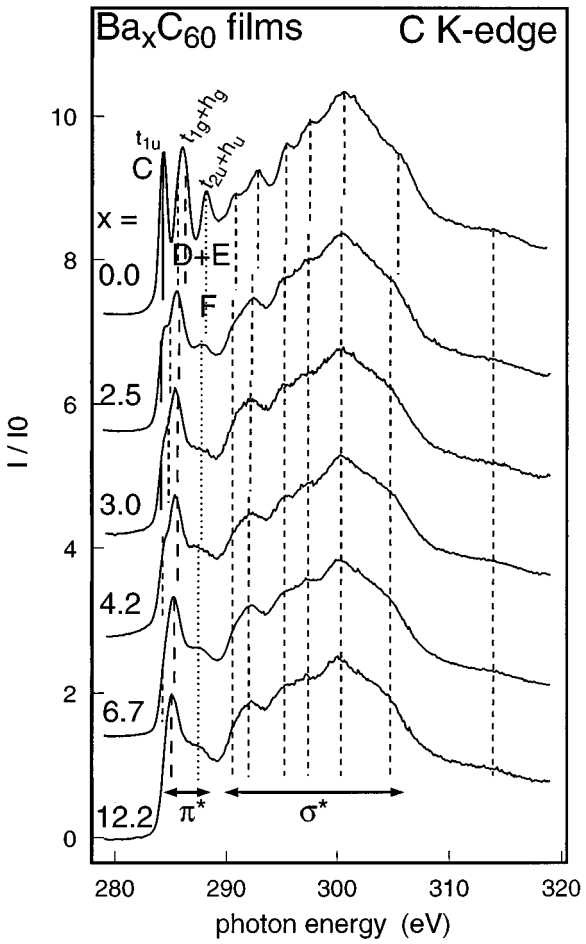

FIG. 5. C *K*-edge absorption spectra of the Ba-doped C_{60} films for Ba concentrations ranging from $x=2.5-12.2$. The top curve shows the absorption spectrum of an undoped ~800 Å-thick pristine C_{60} film.

The corresponding C *K*-edge absorption spectra of the fulleride films are shown in Fig. 5. They reveal excitations from the C $1s$ core level into unoccupied C $2p$-derived states. Neglecting the excitonic interaction of the core hole with the excited electron, the absorption spectra show directly the C $2p$-derived unoccupied DOS. There are four $1s\rightarrow\pi^*$-transitions in the upper absorption spectrum of a pristine C_{60} film. The lowest-energy peak at 284.4 eV is the transition from the C $1s$ to the LUMO (t_{lu}) band (labeled *C*). The second feature is due to the C $1s$ transition into the

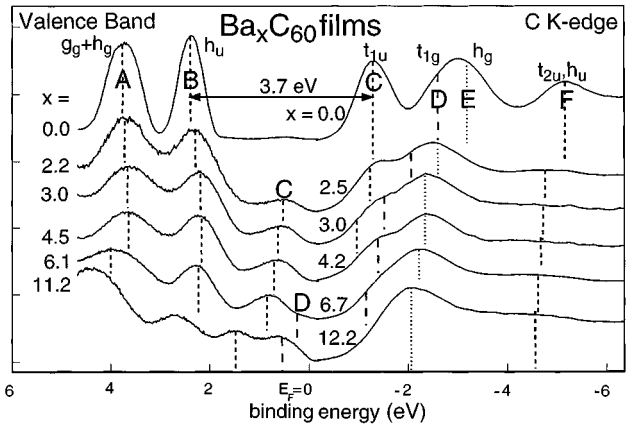

FIG. 6. Photoemission valence-band spectra (left-hand panel) and C *K*-edge absorption spectra (right-hand panel) of the Ba-doped C_{60} films for the same sequence of Ba concentrations ranging between $x=2.2$ and 12.2 as shown in Fig. 5. The top spectra correspond to the pristine C_{60} films. The photon energy scale was transported to the binding-energy scale by using the HOMO (h_u)-LUMO (t_{1u}) gap of the pristine C_{60} film of 3.7 eV. At the lowest Ba concentration of $x=2.2$ or 2.5 the spectra suggest LUMO (t_{1u}) -derived features *C* on both sides of the gap and this band had become filled in $Ba_{(x=3.0)}C_{60}$. The shoulder just at -1.3 eV photon energy in the absorption spectrum of $Ba_{(x=6.7)}C_{60}$ can be attributed to hybrid states involving the LUMO+1 (t_{1g}) band *D*.

LUMO+1 (t_{lg}) (labeled *D*) and LUMO+2 (h_g) (labeled *E*) bands at 285.8 and 286.3 eV, and the third structure at 288.2 eV is assigned to a transition into the LUMO+3, LUMO+4 (t_{2u},h_u) bands (labeled *F*). This has already been observed by x-ray absorption[44] and electron-energy-loss spectroscopy EELS.[11,45,46]

The fulleride-film spectra are in good agreement with the corresponding EELS[11,46] and inverse-photoemission spectroscopy data[15] of the Ca_xC_{60} system with Ca concentrations close to $x=3$ or higher while the spectrum of the film with Ba concentrations close to $x=4.2$ is similar to the spectra of K_6C_{60} and Rb_6C_{60}.[45] The vertical lines should help to identify energy shifts of the C_{60} bands. There are significant changes in the absorption spectra with Ba doping; the initial deposition of Ba causes a shift of all π^* bands towards lower photon energies due to the increasing excess charge on the C_{60} units. Furthermore, the bands are broadened. A closer inspection of the figure shows that the transitions of C 1*s* into the unoccupied σ^* bands above 290 eV photon energy also reveal broadening and small shifting towards lower photon energies. The Ba-doped absorption spectra with concentration of $x=3.0$ and 4.2 are very similar to those of the stage-1 Cs graphite intercalation-compound-absorption data,[47] pointing also to a covalent rather than an ionic type of electronic intercalation of the donor.

A comparison of the occupied valence-band data (left-hand panel), with the corresponding C *K*-edge absorption spectra (right-hand panel) of the fulleride films is given in Fig. 6. The photon energy scale was transported to the BE scale by using the HOMO (h_u)-LUMO (t_{lu}) gap of the pristine C_{60} film of 3.7 eV (center-to-center energy for ($N\pm1$) solid C_{60} systems[12]). At the lowest Ba concentration of $x=2.5$, the spectra of the unoccupied and occupied bands suggest LUMO (t_{lu})-derived features *C* on both sides of the gap. As the Ba content is further enhanced ($x=3.0$), the unoccupied LUMO (t_{lu}) band *C* is decreased while the occupied band intensity is simultaneously increased. Given the evolution of valence bands, it can be concluded that the LUMO (t_{lu}) band *C* has become occupied for a Ba concentration of $x=3.0$, in good agreement with the band-structure model of Sec. IV B. The shoulder at -1.3 *eV* BE for Ba concentration of $x=6.7$ is due to hybrid states involving the LUMO+1 (t_{1g}) -derived band *D*. The filling of this LUMO+1 (t_{1g}) band *D* appears to be complete at Ba concentrations of $x=6.7$.

For the alkaline-earth fullerides, pure ionic-bond formation requires the transfer of two *s* electrons. Theoretical considerations based on the ionization energies of alkaline-earth metals, the electron affinity of C_{60}, and the electrostatic (Madelung) energy of the crystal, demonstrate that such a two-electron transfer is *not* favorable.[12] Therefore, bonding must involve hybridization of C_{60} π^* states and Ba states, as observed, for example, in the graphite-intercalation systems.[48] It is shown in the band-structure Section (IV B) that the Ba atoms are away from the limit of complete charge transfer as a consequence of the competition between covalent Ba-C_{60} bonding and ionic contributions. In Ref. 42 we have shown that covalent admixtures to the Ba-C two-center energy in Ba_3C_{60} are found to be $\sim$75%, while the classical electrostatic Coulomb part contributes $\sim$25%. In Ba_6C_{60} the covalent contribution is reduced to 50% while the Coulomb portion is enhanced to $\sim$50%. This is also supported by recent local-density approximation models of the electronic band structure of Ba_6C_{60},[13,14] where an incomplete charge transfer from the Ba atoms to the C_{60} molecules has been found. This has been interpreted by a hybridization between the $5d$-$6s$ states of the Ba^{1+} ion and the C_{60}-π^* states. Furthermore, the Ba admixtures to the bands are not restricted to a rather narrow region in the vicinity of ε_F, as discussed in the band-structure section. We predict Ba amplitudes in an energy window of almost 10 eV on both sides of ε_F. In contrast to the assumption of a rigid-band model with purely ionic character, this would account for the lower LUMO+1 (t_{1g}) photoemission intensity at Ba concentrations of $x\cong6.1$.

Nevertheless, we have estimated the intensities of the HOMO$-$1 (g_g+h_g), HOMO (h_u), LUMO (t_{1u}), and LUMO+1 (t_{1g}) -derived bands $A-D$ by fitting each with a Gaussian function for all investigated Ba_xC_{60} films. For $x=3.0$, the LUMO-HOMO ratio was $\sim$0.3 (theoretical ratio within a rigid-band model: 0.6), for $x=4.5$ their ratio was 0.4, a value smaller than the ratio of $\sim$0.45 for Ca_3C_{60} (Ref. 15) and $\sim$0.56 for K_6C_{60}.[12] Furthermore, for Ba concentrations of $x=6.1$, 8.6, 10.5, and 11.2 we found LUMO-HOMO ratios of 0.53, 0.50, 0.61, and 0.76. The (LUMO+1)-HOMO ratios were 0.02, 0.05, 0.15, and 0.40 (theoretical ratio: 0.6). This indicates that the Ba atoms can be considered formally as singly ionized. Therefore, an estimation of the number of electrons donated by Ba into the unoccupied bands of the C_{60} molecule cannot be justified under these electronic conditions. Any fitting of the bands with a Gaussian function within the rigid-band model becomes invalid.

TABLE III. Atomic net charges of Ba and C_{60} excess charges in the Ba_xC_{60} series according to INDO CO calculations in the framework of a Mulliken population analysis. The numbers in parentheses symbolize the multiplicity of the corresponding Ba atoms. In $Ba_5C_{60}(2)$ the mean-value averaged over all Ba atoms has been given.

System	Ba net charge	C_{60} excess charge
Ba_3C_{60}	1.119(3)	−3.357
Ba_4C_{60}	1.214(2)	−4.882
	1.227(2)	
$Ba_5C_{60}(1)$	1.131(4)	−5.675
	1.151(1)	
$Ba_5C_{60}(2)$	1.274(5)	−6.370
Ba_6C_{60}	1.309(6)	−7.854

High Ba concentrations up to $x \approx 12$ within the fulleride films, which can only be prepared with the UHV film-deposition technique after the annealing of the films at 620 K for 15 min indicates the formation of a thermodynamically stable Ba-C_{60} solid-state solution. This strongly suggests an incomplete Ba-to-C_{60} charge transfer (CT) as a consequence of the quantum-chemical nature of the Ba-C_{60} interaction. As theoretically predicted, the C_{60} excess electron charge in Ba_6C_{60} is −7.854 (see Table III), which leads to an electron transfer of 1.309 from each Ba atom. Furthermore, it was found that the C_{60} unit has a high ability to accommodate excess electrons. In systems with up to 12 excess electrons on the soccer ball, any sizable weakening of the overall π bonding is prevented.[42] This strongly indicates that the preparation of thermodynamically stable solid-state solutions with Ba concentrations of up $x \approx 12$ are feasible since the Ba atoms in the fullerides are essentially monovalent as a result of the competition between covalent and ionic Ba-C interactions.

B. Band structures

We start the discussion of the INDO CO results of the Ba_xC_{60} fullerides with an analysis of dispersion curves $\varepsilon_i(\mathbf{k})$. In Figs. 7–11 the corresponding energy bands are portrayed in the outer valence region between −15 and −3 eV. We predict a gap in four of the five Ba_xC_{60} solids. A metallic configuration is derived for $Ba_5C_{60}(1)$ only, i.e., that Ba_5C_{60} structure which has been extrapolated from the lighter Ca_5C_{60} homologue. In this context we should emphasize that Ca_5C_{60} has a high-temperature metalic ground-state which transforms into a low-temperature superconducting one.[9] But before discussing the individual $\varepsilon_i(\mathbf{k})$ diagrams, a conceptual advantage of the present CO method should be mentioned. In contrast to the majority of other band-structure approaches, the definition of an internal-energy standard in each calculation is not required in the INDO CO formalism employed. It seems to be a general disadvantage of many band-structure methods that a comparison of absolute band energies and their modifications within a series of related solids is not possible because each calculation leads to a new internal-energy standard for the one-electron energies $\varepsilon_i(\mathbf{k})$. In the present method all one-electron energies are defined in absolute numbers; see Ref. 19. In short, the INDO-based $\varepsilon_i(\mathbf{k})$ curves do not depend on internal-energy standards. It is thus straightforward to analyze modifications in the one-electron energies as a function of the Ba-to-C_{60} CT and the crystal structure on the basis of a common energy zero.

For Ba_3C_{60} we calculate a forbidden gap of about 2.2 eV with the highest-filled band states located at −6.47 eV. They are derived from the molecular LUMO (t_{1u}) orbital. As emphasized in the preceding section this classification is only a formal one as the metal-C_{60} hybridization is rather strong. Thus, any rigid-band model corresponds to an oversimplification. In Ba_xC_{60} fullerides ($x>0$), the LUMO-derived states are occupied as a result of the Ba-to-C_{60} CT. It is well

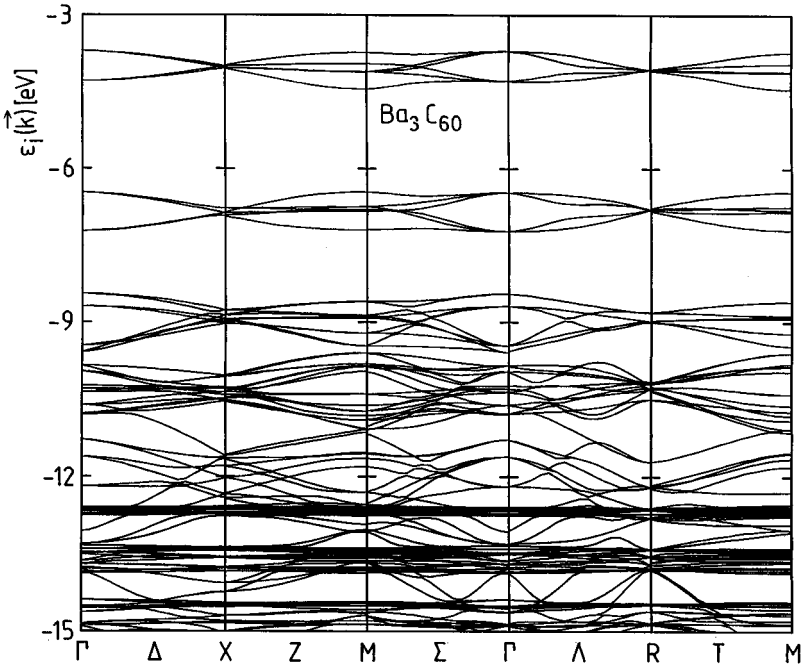

FIG. 7. Energy bands $\varepsilon_1(\mathbf{k})$ of Ba_3C_{60} in the outer valence region between −15 and −3 eV according to INDO CO calculations.

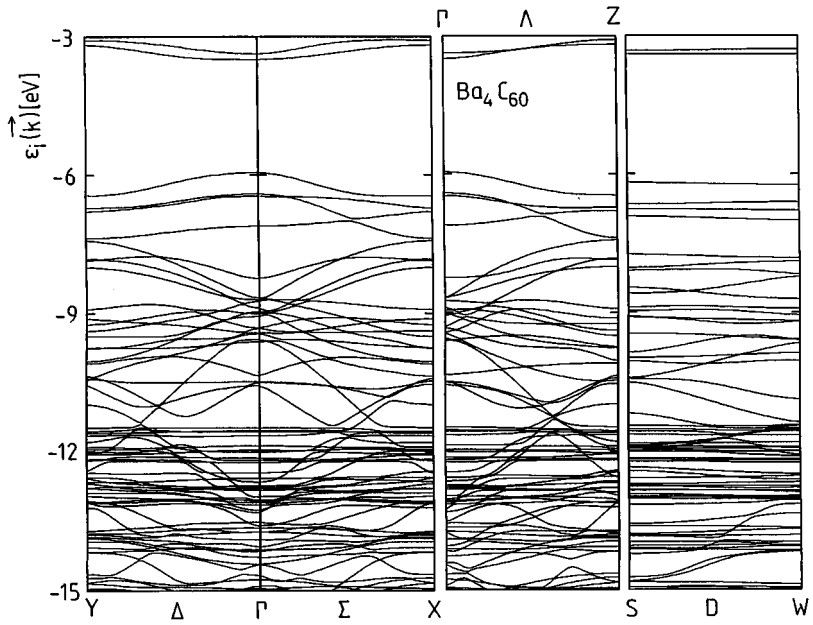

FIG. 8. Energy bands of Ba_4C_{60}.

known that forbidden gaps are always overestimated by methods derived in the framework of the Hartree-Fock approximation.[49] Note, however, that the gap is frequently underestimated in density-functional approaches.[50,51] It can be expected that the ''true'' gap in Ba_3C_{60} occurs in an interval between 0.7 and 1.0 eV. The $\varepsilon_i(\mathbf{k})$ curves in Fig. 7 show a clear discrimination between C_{60} states of π and σ character. The σ bands are rather narrow as a result of the small intermolecular C_{60}-C_{60} overlap. In Ba_3C_{60} these one-electron states are found below -12.6 eV. The filled LUMO band is predicted about 2 eV above the HOMO states derived from the bare C_{60} unit (center of gravity). In the molecular I_h symmetry, these HOMO states transform according to the irreducible representation h_u. The calculated energy separation between the two highest-filled band states of Ba_xC_{60} (=HOMO-LUMO separation if the one-electron states are expressed in terms of the one-electron states of bare C_{60}) of 2 eV is in good agreement with the results of the photoemission measurement; see Sec. IV A. Photoemission spectra of Ba_xC_{60} films with $x \cong 2.2$ have shown that Ba doping leads to a new band located about 1.6 eV above the HOMO peak of undoped C_{60}. The difference of 0.4 eV between theory and experiment is probably caused by many-body corrections that differ in the HOMO and LUMO region of C_{60}. A recent theoretical analysis on the basis of the Green's-function method has shown that many-body corrections for hole states are larger than corrections for the LUMO.[52] As demonstrated in Ref. 52 these many-particle corrections reduce the calculated-energetic splitting between the HOMO and LUMO energies.

Let us come back to the highest-filled bands of Ba_3C_{60}. Figure 7 shows that the six one-electron states (note that we have two formula units Ba_3C_{60} per unit cell) are degenerate only at the R point with fractional coordinates 0.5, 0.5, 0.5. A quasidegeneracy occurs at the X point (fractional coordinates: 0, 0.5, 0). At the Γ point, two one-electron states with threefold degeneracy occur. They correspond to the all-in-

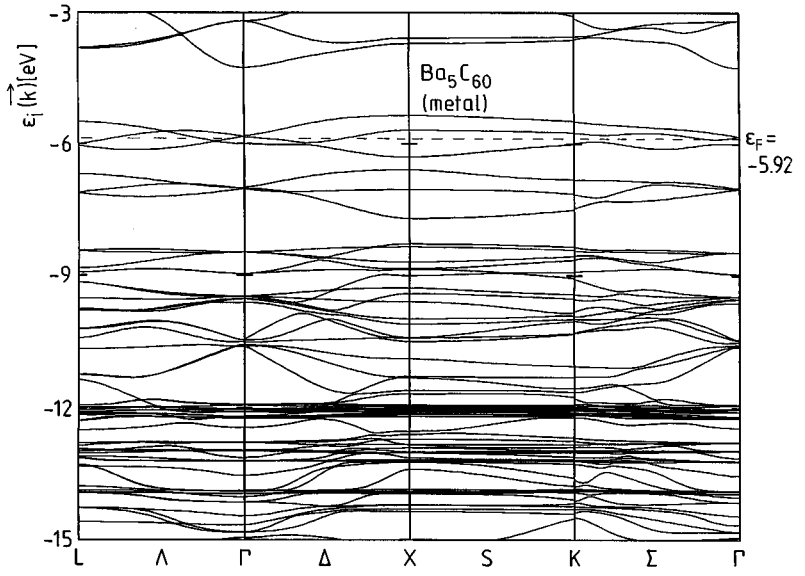

FIG. 9. Energy bands of $Ba_5C_{60}(1)$ in a metallic configuration; ε_F symbolizes the Fermi energy. The bands of the Mott-like state do not differ sizeably from the dispersions shown here.

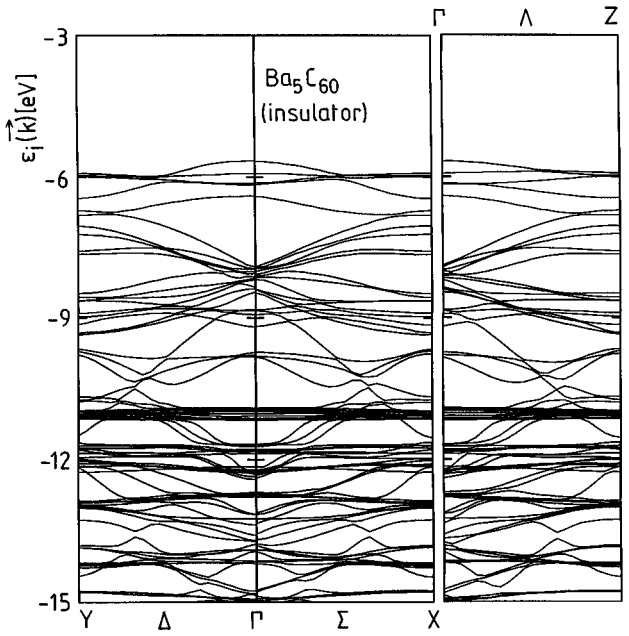

FIG. 10. Energy bands of $Ba_5C_{60}(2)$.

phase and all-out-of-phase combination of the molecular t_{1u} descendant. Their splitting amounts to about 0.75 eV.

The $\varepsilon_i(\mathbf{k})$ curves of Ba_4C_{60} are displayed in Fig. 8. The calculated forbidden gap of this fulleride system is slightly larger than the one observed in Ba_3C_{60}. The lower crystal symmetry with two types of Ba positions leads to a larger splitting of the one-electron states. Figure 8 shows that the nearly dispersionless σ bands do not exhibit such pronounced energetic degeneracies as encountered in the cubic Ba_3C_{60} system. Comparison of the two $\varepsilon_i(\mathbf{k})$ diagrams demonstrates an overall shift of the Ba_4C_{60} energy levels to smaller binding energies. The highest-filled band states of Ba_4C_{60} are predicted slightly above -6 eV. This shift in the CO basis energies of Ba_4C_{60} relative to Ba_3C_{60} to smaller binding energies is even more pronounced for the σ bands. The highest-filled σ dispersions in Ba_4C_{60} are predicted at about -11.6 eV while they are found at about -12.6 eV in Ba_3C_{60}.

The dispersion curves of the two Ba_5C_{60} structures are shown in Figs. 9 and 10. In Fig. 9 we have displayed the $\varepsilon_i(\mathbf{k})$ diagram of $Ba_5C_{60}(1)$ in a metallic configuration with the Fermi energy ε_F at about -5.92 eV. ε_F cuts three energy bands which are derived from the molecular (LUMO+1) states of t_{1g} symmetry. Remember that the LUMO states of t_{1u} symmetry are completely filled by six electrons. In Ba_5C_{60} we are then left with four additional valence electrons leading to a partial occupation of the molecular (LUMO+1) states. In alkali-doped A_3C_{60} fullerides such a many-band crossing of the Fermi energy is suggested as an enhancement factor for the superconducting pairing.[24,53] The delocalization of the Cooper pairs over more than one band leads to an increasing coupling strength. We suggest that the same mechanism is operative in superconducting Ca_5C_{60} which crystallizes in the solid-state structure adopted for $Ba_5C_{60}(1)$. Test calculations with the present INDO CO approach have shown that the overall shape of the band structure displayed in Fig. 9 is conserved for Ca_5C_{60}. Many-band scattering with Cooper-pair delocalization over three bands should be accessible in this Ca fulleride. The INDO CO calculation leads to an electronic DOS at ε_F $[=N(0)]$ of about 8.4 states per eV, a value that is somewhat smaller than $N(0)$ elements extrapolated or calculated in alkali-doped C_{60} fullerides.[40] This difference between alkali- and alkaline-earth-doped fullerides can be traced back to the smaller-unit-cell dimensions realized in alkaline-earth-doped materials. The overall width $\Delta\varepsilon$ of the $Ba_5C_{60}(1)$ conduction band is roughly 1 eV. Recent theoretical works in different degrees of sophistication have shown that the so-called (intramolecular) Hubbard two-electron repulsion U in bare C_{60} is larger than the $\Delta\varepsilon$ value of $Ba_5C_{60}(1)$ by a factor of 3 to 4.[25,54–56] In doped fullerides U and $\Delta\varepsilon$ are of the same order of magnitude; here the Hubbard U is reduced to values between 0.7 and 1.0 eV.[24,25] But then one has to expect a strong competition between a metallic ground state and an

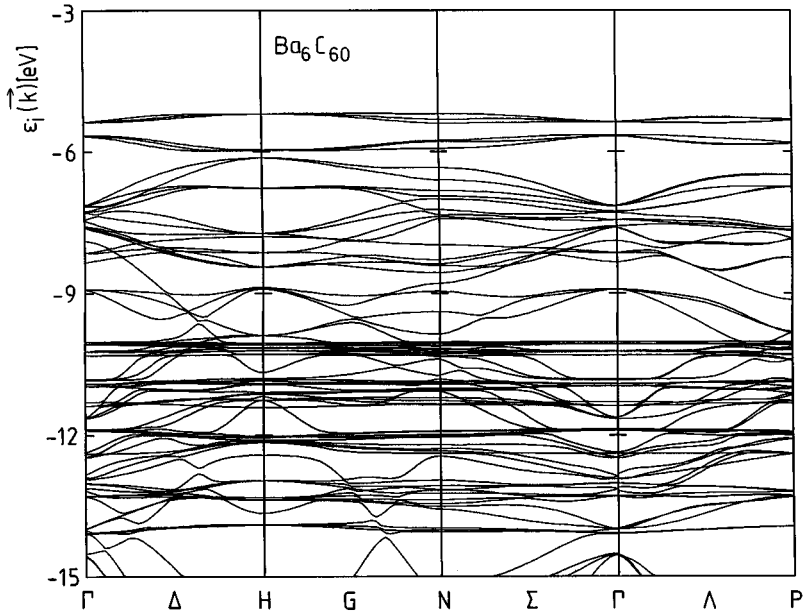

FIG. 11. Energy bands of Ba_6C_{60}.

insulating Mott-like state with a maximum number of singly occupied **k** microstates in the highest-filled band(s). In the one-determinantal approximation of the present CO approach, we predict an almost perfect energetic degeneracy between both configurations. We feel that the CO results derived for $Ba_5C_{60}(1)$ are in line with experimental observations in many alkali- and alkaline-earth-doped fullerides, which have shown that even minor electronic modifications (i.e., doping center, unit-cell dimension) are sufficient to cause transitions between both types of electronic configurations.[20,21]

The energy bands of $Ba_5C_{60}(2)$ are displayed in Fig. 10. For this Ba_5C_{60} solid-state arrangement, an insulating ground state with a forbidden gap of about 3 eV is predicted. Again we expect that the ''true'' gap amounts to 1.0–1.5 eV. Comparison of Figs. 9 and 10 indicates that both $\varepsilon_i(\mathbf{k})$ diagrams differ remarkably. The width of the π-type functions in the insulating modification $Ba_5C_{60}(2)$ exceeds the width of the π-type dispersions realized in $Ba_5C_{60}(1)$. It seems that the bonding interaction of the Ba atoms to the C_{60} soccer balls is less efficient in the fcc phase with its Ba_4 tetrahedron on the interstitial *o* site. The absolute band energies in Figs. 9 and 10 indicate that most of the one-electron states of the metallic configuration are found at lower energies. Here the highest-occupied C_{60} σ-like states occur at about -12 eV while they are found at about -11 eV in Ba_5C_{60}. (2) The electronic origin of this relative shift of one-electron levels in isoelectronic solids will be explained below. We have already mentioned that both suggestions of solid-state structures are affected by some unavoidable uncertainties. Therefore, a quantitative comparison of the total energies of the two Ba_5C_{60} models is not possible. Nevertheless, we have observed that the insulating structure, i.e., $Ba_5C_{60}(2)$, is of lower energy than the metallic structure $Ba_5C_{60}(1)$. This energetic graduation is in line with the strength of the Ba-C_{60} interaction discussed in connection with the dispersion curves displayed in Figs. 9 and 10. It seems that Ba_5C_{60} and Ca_5C_{60} prefer different solid-state arrangements. The completely different behavior of both AE_5C_{60} fullerides (AE = Ca,Ba) remember that Ca_5C_{60} is a superconductor, and can be considered as an outcome of these different preferences in the solid-state structure.

Finally, we consider the energy bands of Ba_6C_{60} where the molecular t_{1u} LUMO and t_{1g} (LUMO+1) states are filled completely by twelve electrons. Figure 11 shows that the energetic splitting between both groups of energy bands is rather small. This is in line with the photoemission data where the two peaks derived from the molecular t_{1g} and t_{1u} orbitals (see Figs. 3 and 4) collapse into a common one. The highest-filled states occur at about -5.2 eV. As an overall effect, we have a continuous shift of the $\varepsilon_i(\mathbf{k})$ numbers to higher orbital energies with increasing Ba doping. In Ba_6C_{60} the highest-filled σ dispersions are predicted at about -10 eV. Furthermore, the $\varepsilon_i(\mathbf{k})$ diagram indicates that the energy bands derived from the molecular t_{1u} and t_{1g} orbitals are degenerate at the Γ, H, and P points. H and P have fractional coordinates 0, 0.5, 0 and 0.25, 0.25, 0.25. At other symmetry points and in all symmetry directions this degeneracy is lifted. Comparison of the five $\varepsilon_i(\mathbf{k})$ plots of Figs. 7–11 indicates that such degeneracies of the one-electron levels in reciprocal space only occur in the two cubic solids Ba_3C_{60} and Ba_6C_{60}. But even here, the highest degeneracy compatible with the crystal symmetry is threefold. Band states that are derived from molecular levels with fourfold and fivefold degeneracy are split even at the symmetry points mentioned above for both cubic lattices.

We feel that it is necessary to relate the Ba_6C_{60} band-structure results together with the photoemission data on one side, to the superconductivity assigned to Ba_6C_{60}, on the other.[10] According to the present CO calculations, Ba_6C_{60} is an insulator with a forbidden gap of about 4.5 eV. We have mentioned above that the present Hartree-Fock-based approximation tends to overestimate band gaps. But a recent density-functional study known to underestimate the gap predicts an insulating band structure as well.[14] Photoemission spectroscopy yields an insulating state for Ba_xC_{60} for $x = 4.5 \pm 0.7$ and a semimetallic state for $x = 6.1 \pm 0.9$. The uncertainties in the stoichiometry prevent a clear experimental answer to the question whether or not Ba_6C_{60} is metallic. But a nonmetallic state is probably compatible with the spectroscopic results. On the basis of the density-functional study of Ref. 14 and the present CO calculations, the exact stoichiometry of the superconducting Ba fulleride seems to be questionable. We believe that Ba_6C_{60} is *not* the stoichiometry of the superconducting phase. By analogy with Ba_3C_{60}, we have studied the band-structure properties of other Ba_6C_{60} solid-state geometries as well. We have adopted structures compatible with a bcc lattice (space-group symmetries Im3m, Im3, variation of the unit-cell dimension). Despite these additional degrees of freedom, a gap between filled and unfilled dispersion curves survived in all band-structure realizations.

Next we discuss the DOS profiles of the five solids. The corresponding diagrams have been collected in Fig. 12 in the valence region between -30 and 0 eV. The DOS profile of undoped C_{60} is more or less conserved in Ba_3C_{60}. Note that the undoped fullerene crystallizes in high cubic fcc symmetry. The Ba_3C_{60} and C_{60} DOS distributions differ with respect to the peaks assigned as *a* and *b* in Fig. 12. Peak *a* is caused by the aforementioned LUMO band (t_{1u} symmetry in the C_{60} molecule) which is occupied by six electrons and peak *b* has its origin in hybridized t_{1g} states. The two maxima on the high-energy side of peak *a* are caused by C_{60} π functions of h_u (first maximum) and h_g, g_g (second maximum) symmetry. In cubic-fulleride crystals these ''molecular fingerprints'' of π states are conserved in the solid state. The symmetry reduction in Ba_4C_{60} to an orthorhombic Bravais lattice is accompanied by a remarkable perturbation in the DOS structure in the outer valence region. The fcc symmetry of $Ba_5C_{60}(1)$ restores the DOS profile realized in Ba_3C_{60}. The energetic separation between peaks *a* and *b* (t_{1u} and t_{1g} descendants), however, is reduced as a result of the partial t_{1g} occupation. This variation of the DOS maxima is even enhanced in Ba_6C_{60}, where the t_{1g}-derived states (= peak *b* in Fig. 12) are fully occupied. In analogy to Ba_4C_{60} the low symmetry of $Ba_5C_{60}(2)$ causes perturbations in the DOS profile in the outer valence region relative to the common DOS pattern encountered in all cubic fullerides. We wish to point out that the calculated DOS profiles reproduce the photoemission data in the extreme outer valence region which have been discussed in the photoemission section

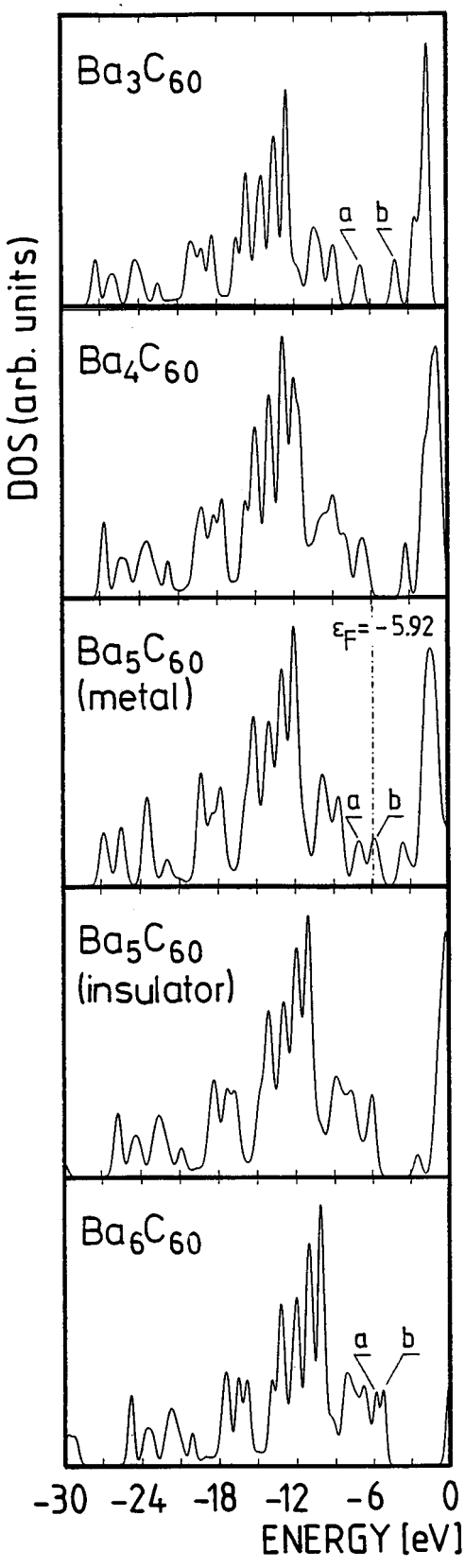

FIG. 12. Calculated electronic density-of-states distribution of Ba_xC_{60} fullerides in the valence region between -30 and 0 eV. With the exception of Ba_3C_{60}, with $z=2$, all DOS curves have been renormalized with a common scale factor (arbitrary units). The Fermi energy ε_F of $Ba_5C_{60}(1)$ is indicated. The origin of the peaks labeled *a* and *b* is explained in the text.

(Sec. IV A). In the UPS spectra of the Ba_xC_{60} fulleride films, four peaks are clearly resolved. They are associated with the C_{60} π states of g_g, h_g, and h_u symmetry and the π^* LUMO and (LUMO+1) states of t_{1u} and t_{1g} symmetry. The CO approach predicts that the energetic separation between the g_g, h_g, and h_u -based peaks and the t_{1u}, t_{1g} ones is reduced with increasing doping. This theoretical result is in line with the photoemission data. Figure 12 is a convenient representation for visualizing the shift of the one-electron energies in Ba_xC_{60} as a function of the alkaline-earth doping.

As a final theoretical topic, we analyze the magnitude of the Ba-to-C_{60} CT and thus the quantum chemical nature of the Ba-C_{60} interaction. In Table III we have collected the net charges of the Ba atoms as well as the excess charge on the C_{60} unit in the alkaline-earth-doped fullerides studied. The net charges in the table are based on a Mulliken population analysis.[57] We are aware of the difficulties in calculating atomic net charges at electropositive centers with diffuse orbitals. In this context we refer to Ref. 14, where it has been shown that the Ba-to-C_{60} CT in Ba_6C_{60} is incomplete, independent of the details of the procedure used to estimate the atomic charges. In the density-functional work, both a Mulliken population analysis as well as a volume integration has been employed. In any case, we want to emphasize that atomic net charges do not have the character of an expectation value, but that they are a useful auxiliary quantity to discuss electronic-structure properties on the basis of computational quantities that have a well-defined physical meaning. In Table III, it is seen that the Ba atoms are far away from the limit of complete valence CT which would lead to a Ba net charge of 2.0. According to the present CO model slightly more than one electron per Ba atom have been transferred to the C_{60} molecule. With increasing Ba concentration, the CT is enhanced. In the Ba_xC_{60} fullerides one has a competition between covalent Ba-C_{60} bonding and ionic contributions. The variation of the Ba net charges emphasizes that the importance of ionic contributions to the binding of Ba is enhanced with increasing doping. This result can be quantified by calculating the interaction energy between a Ba atom and the nearest C atom of the C_{60} unit. In Ref. 26 we have shown that covalent (hopping) admixtures to the Ba-C two-center energy in Ba_3C_{60} are found between 72 and 79%, while the classical electrostatic Coulomb-part contributes 19–26%. In Ba_6C_{60} the Coulomb contribution to the Ba-C two-center energy is enhanced to about 47%. The covalent contributions are reduced to about 51%. The exchange interaction contributes only a small amount to the net two-center energy. In Ba_6C_{60} we have the situation that the Ba-C interaction contains almost the same amount of covalent and ionic admixtures. As already mentioned, a rigid-band model cannot be justified under these electronic conditions. Nevertheless, it is important to mention that the Ba admixtures to the CO wave functions are not restricted to a narrow region in the vicinity of ε_F (see above). Nonnegligible Ba amplitudes are predicted in an energy window of several eV on both sides of ε_F. This information may be important for the discussion of superconducting pairing mechanisms. In the case of an electron-phonon coupled mechanism, the isotope effect caused by the doping atom would be much smaller than expected on the basis of the theoretically derived charge distribution under the assumption that the transferred elec-

trons occupy states near the Fermi energy. The calculated shifts of the one-electron energies in the Ba_xC_{60} series are easy to explain via the charge distribution given in Table III. With an increasing excess charge on the C_{60} soccer ball, the Ba_xC_{60} one-electron energies are shifted to less negative $\varepsilon_i(\mathbf{k})$ values for the occupied bands. The difference in the center of gravity of the energy bands of the two Ba_5C_{60} structures is caused by the different Ba-to-C_{60} CT in both solid-state arrangements.

Obviously, the π electronic structure in the C_{60} unit must be modified as a result of the Ba-to-C_{60} CT. An analysis of so-called Wiberg bond indices[58] shows that the discrimination between carbon-carbon double (6-6) and single (6-5) bonds is attenuated with an increasing concentration of alkaline-earth dopants. A detailed investigation of this topic will be left for a future contribution. The most important result is as follows.

In bare C_{60} the (6-6) bonds show a sizeable double-bond character, while the (6-5) bonds are essentially C-C single bonds. In Ba_6C_{60} this relative graduation is reversed. Here the double-bond character of the (6-6) bonds is smaller than that of the (6-5) bonds. Of course this charge-dependent modification of the double-bond character of the (6-6) and (6-5) bonds must be accompanied by a reduction in the maximum value of the Wiberg indices. Note that the number of (6-5) bonds exceeds the number of (6-6) bonds by a factor of 2. The calculated modification of the bond character as a function of increasing doping leads to an enhancement of the double-bond character in the majority component of the C-C bonds and to a simultaneous reduction in the minority component. As an overall effect we find that the mean value of the bond index is more or less independent of the concentration of Ba atoms. We have already suggested that the increasing widths of the photoemission peaks with increasing doping are caused by increasing amplitudes of the zero-point vibrations in the C_{60} unit in the presence of electronic excess charges (enhanced Coulomb repulsion) and reduced maxima in the bond indices measuring covalency. In recent theoretical publications, it has been shown that the amplitudes of these zero-point vibrations exceed 0.07 Å already in the undoped C_{60} fullerene with the aforementioned clear discrimination between (6-6) double and (6-5) single bonds.[59,60] Of course, this broadening of the photoemission peaks has not been reproduced by the CO calculations based on a fixed C_{60} soccer ball geometry. But the conservation of a common fulleride geometry allowed us to study the charge-induced modification of the π electronic structure in the absence of any intramolecular geometric degrees of freedom. With increasing doping one expects an increasing C_{60} diameter and a decreasing bond-length alternation.

V. CONCLUSIONS

The photoemission and the XAS spectra of the Ba-doped C_{60} fulleride films indicate that Ba_xC_{60} films are semiconductors or insulators for Ba concentrations of up to $x \approx 4.5$ (± 0.7). They probably become semiconductors for Ba concentrations of $x \approx 6.1$ (± 0.9) and a semimetal or metal for Ba concentrations of $x > \sim 6.1$ due to the filling of the LUMO+1 (t_{1g})-derived band crossing the Fermi level. In the case of Ba_5C_{60}, the CO calculations on the basis of two plausible solid-state geometries lead to an insulating and a metallic electronic configuration. Both geometries differ in the spatial arrangement of the Ba atoms. The metallic state is quasidegenerate with a Mott-like insulator. Additionally, the present CO calculations indicate that the exact stoichiometry of the superconducting Ba fulleride phase seems to be questionable yet. We have observed lower photoemission of the LUMO (t_{1u}) and LUMO+1 (t_{1g}) -derived bands in the fulleride films at all Ba concentrations considered as theoretically predicted under the assumption of a purely ionic character of the Ba-C interaction within a rigid-band model. This strongly indicates that the Ba atoms are away from the limit of complete charge transfer. In the Ba-doped fullerides one has strong competition between covalent and ionic Ba-C_{60} bonding. This is in contrast to the interpretation of Ca and Ba fullerides in Refs. 17 and 46, where one has assumed complete alkaline-earth-to-C_{60} CT for doping levels of up to $x = 3$ and a nonrigid band behavior together with partial filling of the LUMO+1 (t_{1g}) -derived band for higher doping levels. Our theoretical results strongly suggest that the electronic structure of the fulleride system for all Ba concentrations is characterized by a strong hybridization of the Ba atoms with the π-type functions of the C_{60} network. This is again in contrast to the interpretation of the nonrigid-band behavior for the Ca-fulleride system,[46] where reduced energy separation of the C_{60} molecular orbitals caused by a decreased dimerization of C_{60} upon n-type doping has been assumed. The formation of highly-doped Ba-C_{60} fulleride films with concentrations of up to $x \approx 12$ with the UHV film deposition technique is feasible as a consequence of the incomplete Ba-to-C_{60} CT, and, furthermore, it proceeds from the significant ability of C_{60} to accommodate up to 12 excess electrons.

ACKNOWLEDGMENTS

This work was supported by the Bundesministerium für Bildung und Forschung through its fullerene project and by the Fonds der Chemischen Industrie. One of us (Th.Sch.) thanks Professor A. M. Bradshaw, Fritz-Haber-Institut der MPG, for helpful discussions and financial support.

*Author for correspondence: Fritz-Haber-Institut der Max-Planck-Gesellschaft, Faradayweg 4-6, D-14195 Berlin (Dahlem), Germany. FAX: ++49-30-8413-4401. Electronic address: thomas@carbon.rz-berlin.mpg.de

[1] R. C. Haddon, Acc. Chem. Res. **25**, 127 (1992).

[2] A. Raghunathan, Supercond. **6**, 1 (1993).

[3] *Buckministerfullerenes*, edited by W. E. Billups and M. A. Ciutolini (VCH, Weinheim 1993).

[4] *Solid State Physics*, edited by H. Ehrenreich and F. Spaepen (Academic, Boston, 1994), Vol. 48.

[5] J. Rosseinsky, D. W. Murphy, R. M. Flemming, R. Tycko, A. P. Ramirez, T. Siegrist, G. Dabbagh, and S. E. Barrett, Nature **356**, 416 (1992).

[6] T. Tanigaki, I. Hirosawa, T. W. Ebbesen, J. Mizuki, Y. Shimakawa, Y. Kubo, J. S. Tsai, and S. Kuroshima, Nature **356**, 419 (1992).

[7] K. Holczer, O. Klein, S.-M. Huang, B. Kaner, K.-J. Fu, R. L. Whetten, and F. Dieterich, Science **252**, 1154 (1991).

[8] C.-C. Chen, S. P. Kelty, and C. M. Lieber, Science **253**, 886 (1991).
[9] A. R. Kortan, N. Kopylov, S. Glarum, E. M. Gyorny, A. P. Ramírez, R. M. Flemming, F. A. Thiel, and R. C. Haddon, Nature **355**, 529 (1992).
[10] A. R. Kortan, N. Kopylov, S. Glarum, E. M. Gyorgy, A. P. Ramírez, R. M. Flemming, O. Zhou, F. A. Thiel, P. L. Trevor, and R. C. Haddon, Nature **360**, 566 (1992).
[11] M. S. Golden, M. Knupfer, J. Fink, J. F. Armbruster, T. R. Cummins, H. A. Romberg, M. Roth, M. Sing, M. Schmidt, and E. Sohmen, J. Phys. Condens. Matter **7**, 8219 (1995).
[12] J. H. Weaver, J. Phys. Chem. **53**, 1433 (1992).
[13] S. Saito and A. Oshiyama, Phys. Rev. Lett. **71**, 121 (1993); Solid State Commun. **83**, 107 (1992).
[14] S. C. Erwin and M. R. Pederson, Phys. Rev. B **47**, 14 657 (1993).
[15] Y. Chen, D. M. Poirier, M. B. Jost, C. Gu, T. R. Ohno, J. L. Martins, J. H. Weaver, L. P. F. Chibante, and R. E. Smalley, Phys. Rev. B **46**, 7961 (1992).
[16] G. K. Wertheim, G. N. E. Buchanan, and J. E. Rowe, Science **258**, 1638 (1992).
[17] M. Knupfer, F. Stepniak, and J. H. Weaver, Phys. Rev. B **49**, 7620 (1994).
[18] Y. Chen, F. Stepniak, J. H. Weaver, L. P. F. Chibante, and R. E. Smalley, Phys. Rev. B **45**, 8845 (1992).
[19] R. Ramírez and M. C. Böhm, Int. J. Quantum Chem. **34**, 47 (1988).
[20] F. Stepniak, P. J. Benning, and J. H. Weaver, Phys. Rev. B **48**, 1899 (1993).
[21] R. C. Haddon, A. S. Perel, R. C. Morris, S.-H. Chang, A. F. Fiory, F. F. Hebard, T. M. Palstra, and G. P. Kochanski, Chem. Phys. Lett. **218**, 100 (1994).
[22] *Practical Surface Analysis*, edited by D. Briggs and M. P. Seah, 2nd ed. (Wiley, Chichester, 1990), Vol. 1.
[23] J. Schulte and M. C. Böhm, Solid State Commun. **93**, 249 (1995).
[24] M. C. Böhm and J. Schulte, Physica C **252**, 282 (1995).
[25] M. C. Böhm and J. Schulte, Mol. Phys. **87**, 735 (1996).
[26] M. C. Böhm, Th. Schedel-Niedrig, H. Werner, R. Schlögl, and J. Schulte, Solid State Commun. **98**, 463 (1996).
[27] R. Ramírez and M. C. Böhm, Z. Naturforsch. Teil A **42A**, 1346 (1987).
[28] R. Ramírez and M. C. Böhm, Int. J. Quantum Chem. **34**, 73 (1988).
[29] M. C. Böhm, Chem. Phys. **128**, 457 (1988).
[30] M. Y. Lavrenziev, H. Köppel, and M. C. Böhm, Chem. Phys. **169**, 85 (1993).
[31] R. Ramírez and M. C. Böhm, Phys. Status Solidi B **135**, 661 (1986).
[32] F. Pfirsch and M. C. Böhm, Chem. Phys. **98**, 89 (1985).
[33] R. A. Evarestov and V. P. Smirnov, Phys. Status Solidi B **119**, 9 (1983).
[34] R. Ramírez and M. C. Böhm, Int. J. Quantum Chem. **34**, 571 (1988).
[35] S. C. Miller and W. F. Love, *Tables of Irreducible Representations of Space Groups and Co-Representations of Magnetic Space Groups* (Pruett, Boulder, 1967).
[36] N. F. Mott, *Metal Insulator Transitions* (Taylor and Francis, London, 1990).
[37] M. C. Böhm, R. Ramírez, and A. M. Oles, Ber. Bunsenges. Phys. Chem. **91**, 717 (1987); Chem. Phys. **117**, 405 (1987).
[38] H. Werner, Ph.D. thesis, Universität Frankfurt, 1995.
[39] A. R. Kortan, N. Kopylov, R. M. Flemming, O. Zhou, F. A. Thiel, R. C. Haddon, and H. M. Raabe, Phys. Rev. B **47**, 13 070 (1993).
[40] W. E. Pickett, in *Solid State Physics*, edited by H. Ehrenreich and F. Spaepen (Academic, Boston, 1994), Vol. 48, p. 226, and references cited therein.
[41] J. P. Axe, S. C. Moss, and D. A. Neumann, in *Solid State Physics*, edited by H. Ehrenreich and F. Spaepen (Academic, Boston, 1994), Vol. 48, p. 149.
[42] M. C. Böhm, Th. Schedel-Niedrig, H. Werner, R. Schlögl, and J. Schulte, Z. Naturforschung. Teil A **51A**, 283 (1996).
[43] D. M. Hill, H. M. Meyer III, and J. H. Weaver, Surf. Sci. **225**, 63 (1990).
[44] L. J. Terminello, D. K. Shuh, F. J. Himpsel, D. A. Lapiano-Smith, J. Stöhr, D. S. Bethune, and G. Meijer, Chem. Phys. Lett. **182**, 491 (1991).
[45] E. Sohmen and J. Fink, Phys. Rev. B **47**, 14 532 (1993).
[46] H. Romberg, M. Roth, and J. Fink, Phys. Rev. B **49**, 1427 (1994).
[47] J. Blöcker, H. Werner, D. Herein, R. Schlögl, Th. Schedel-Niedrig, M. Keil, and A. M. Brashaw, Mater. Sci. Forum **91-93**, 337 (1992).
[48] M. C. Böhm, J. Schulte, and R. Schlögl, Phys. Status Solidi B **196**, 131 (1996).
[49] J. J. Ladik, *Quantum Theory of Polymers as Solids* (Plenum, New York, 1988).
[50] R. A. Heaton, J. G. Harrison, and C. C. Lin, Phys. Rev. B **28**, 5992 (1983).
[51] W. E. Pickett and C. S. Wang, Phys. Rev. B **30**, 4719 (1984).
[52] M. C. Böhm, J. Schulte, and S. Philipp, Chem. Phys. Lett. **226**, 381 (1994).
[53] M. J. Rice, H. Y. Choi, and Y. R. Wang, Phys. Rev. B **44**, 10 414 (1991).
[54] M. R. Pederson and A. A. Quong, Phys. Rev. B **46**, 13 584 (1992).
[55] V. P. Andropov, O. Gunnarsson, and O. Jepsen, Phys. Rev. B **46**, 13 647 (1992).
[56] R. L. Martin and J. P. Ritchie, Phys. Rev. B **48**, 4845 (1993).
[57] R. S. Mulliken, J. Chem. Phys. **23**, 1833 (1955).
[58] K. B. Wiberg, Tetrahedron **24**, 1083 (1968).
[59] J. Kohanoff, W. Andreoni, and M. Parrinello, Phys. Rev. B **46**, 4371 (1992).
[60] R. Ramírez and M. C. Böhm, J. Phys. Condens. Matter **7**, 4847 (1995); M. C. Böhm and R. Ramírez, J. Phys. Chem. **99**, 12 401 (1995).